






## Splitting of fast relaxation in a metallic glass by laser shocks

C. Yang <sup>1,2</sup> J. Duan,<sup>1,2</sup> G. Ding,<sup>1</sup> Y. J. Bai <sup>2,3</sup> B. C. Wei,<sup>2,3</sup> Y. P. Wei,<sup>2,4</sup> S. N. Liu,<sup>5</sup> S. Lan <sup>5</sup>  
B. B. Zhang <sup>6</sup> C. J. Shi,<sup>6</sup> L. H. Dai,<sup>1,2</sup> and M. Q. Jiang <sup>1,2,\*</sup>

<sup>1</sup>State Key Laboratory of Nonlinear Mechanics, Institute of Mechanics, Chinese Academy of Sciences, Beijing 100190, China

<sup>2</sup>School of Engineering Science, University of Chinese Academy of Sciences, Beijing 101408, China

<sup>3</sup>Key Laboratory of Microgravity, Institute of Mechanics, Chinese Academy of Sciences, Beijing 100190, China

<sup>4</sup>Key Laboratory for Mechanics in Fluid Solid Coupling Systems, Institute of Mechanics, Chinese Academy of Sciences, Beijing 100190, China

<sup>5</sup>Herbert Gleiter Institute of Nanoscience, Nanjing University of Science and Technology, Nanjing 210094, China

<sup>6</sup>Beijing Synchrotron Radiation Facility, Institute of High Energy Physics, Chinese Academy of Sciences, Beijing 100049, China



(Received 4 October 2023; accepted 30 November 2023; published 2 January 2024)

Fast relaxation, a locally dynamic activation, universally occurs in metallic glasses below room temperature. Despite much attention, its structural origin has barely been solved and remains mysterious. In this work, the dynamic mechanical relaxations of a typical Zr-based metallic glass with different structural states are systematically studied from 135 to 748 K. We find that the single-peak ( $\beta'$ ) fast relaxation in the annealed glass splits into two distinct peaks ( $\gamma$  and  $\beta'$ ) by multiple-pulse laser shocks, and this dynamics splitting will vanish after re-annealing. Slight structural rejuvenation of the laser-shocked sample is detected by thermodynamic measurements. Structural characterizations further reveal that the laser shocks lead to an increase in the edge-sharing medium-range orders (MROs), which is then recovered by re-annealing. The one-to-one changes in relaxation dynamics and atomic structures provide convincing evidence that the fast relaxation originates from the excitation of MRO structures, and its splitting is due to the reconstruction of MROs. We also find that the split fast relaxations contribute to the room-temperature plasticity of the studied glasses.

DOI: [10.1103/PhysRevB.109.024201](https://doi.org/10.1103/PhysRevB.109.024201)

### I. INTRODUCTION

Relaxation dynamics of glassy matter is probably one of the deepest and most challenging unsolved problems in condensed matter physics. Metallic glasses (MGs) are considered as simple glasses with dense-packed atoms, thus providing an ideal model for studying glassy relaxation [1,2]. Like other glasses, MGs universally exhibit the primary  $\alpha$  relaxation and the secondary  $\beta$  relaxation, and the latter usually serves as a precursor of the former. The  $\beta$  relaxation, associated with the localized stringlike motions of atoms [3], can persist in the glassy state, while the large-scale  $\alpha$  relaxation is almost frozen below the mode coupling temperature. Stress relaxation experiments [4,5] revealed that the frozen  $\alpha$  relaxation will split into a stress-driven fast event, similar to the ballisticlike particle motion probed by x-ray photon correlation spectroscopy [6], and a slow subdiffusive event. In a Al<sub>90</sub>Sm<sub>10</sub>MG, Sun *et al.* [7] discovered an anomalous  $\alpha_2$  relaxation, caused by the mobility decoupling of constituting atoms, that locates between  $\alpha$  and  $\beta$  processes. It is noted that all relaxations mentioned above manifest themselves above room temperature (RT).

In 2015, Wang *et al.* [8] identified a fast relaxation in a La-based MG below RT (at 266 K). Further studies show that such fast relaxations universally exist in MGs at temperatures ranging 0.20–0.55 $T_\alpha$  (the  $\alpha$  relaxation temperature).

They behave either as  $\gamma$  relaxation at around 0.2–0.37 $T_\alpha$  in Zr-based and Pd-based MGs [9], or as  $\beta'$  relaxation at around 0.37–0.55 $T_\alpha$  in La-based and Pr-based MGs [10]. Recently, Shao *et al.* [11] found that the fast  $\gamma$  and  $\beta'$  relaxations can coexist as two peaks in Dy-based MGs. By calculating the activation energy, the activation volume for fast relaxations is suggested to range 0.4–1.3 nm<sup>3</sup> [8–12]. Through molecular dynamics simulations, Wang *et al.* [13] suggested that the fast relaxation originates from the reversible motion of some nearest-neighbor (NN) atoms near 2.5 Å. However, a recent study by Chang *et al.* [14] revealed that the fast relaxation is associated with the stringlike diffusion of the liquidlike atoms beyond the NN scale. Therefore, the structural origin of the fast relaxation is still under debate and needs further careful studies.

In this work, we combine laser shocks and isothermal annealing to modulate the fast relaxations of a Zr-based MG from single- to two-peak, and further detect the corresponding thermodynamic and structural changes. Our results present direct experimental evidence for the structural origin of fast relaxations, that is, the reversible motions of atoms on the MRO scale. The mechanical behaviors of these modulated glasses are also investigated by using nanoindentations.

### II. EXPERIMENT

A bulk Vit105 (Zr<sub>52.5</sub>Ti<sub>5</sub>Cu<sub>17.9</sub>Ni<sub>14.6</sub>Al<sub>10</sub>) MG was chosen for this study due to its pronounced fast relaxation in the range 0.20–0.45  $T_\alpha$  [12,15]. Samples with the dimensions

\*mqjiang@imech.ac.cn

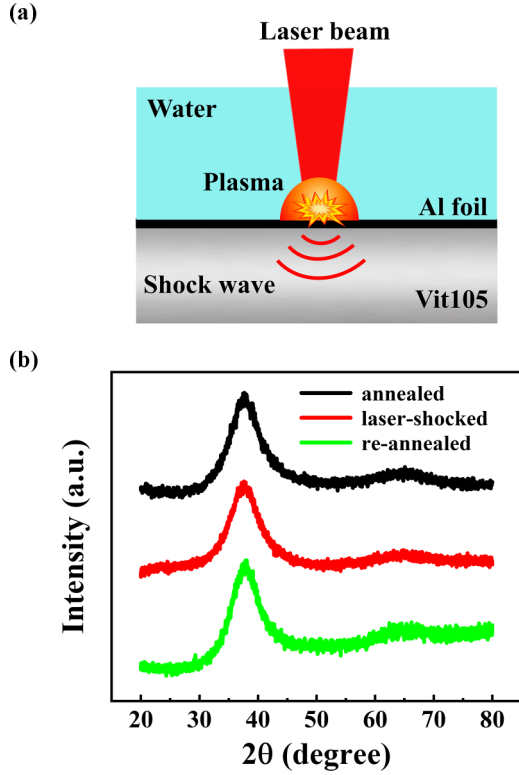


FIG. 1. (a) Schematic illustration of the laser shock treatment on the bulk Vit105 MG sample. (b) XRD patterns of the annealed, laser-shocked, and re-annealed samples.

of  $30 \times 2 \times 1 \text{ mm}^3$  were prepared for dynamic mechanical analyzer (DMA) tests. Before DMA tests, all samples were annealed at 653 K for 12 h to eliminate their thermal history. Some annealed samples were further treated by laser shocks with a  $Q$ -switched Nd:YAG laser operating at a wavelength of 1064 nm. A total of 60 shocks were performed on the top of the specimen in two lines along the length of the sample. Each shock has the output energy of 1.2 J, and its pulse duration is 10 ns. The laser spot has a diameter of 2 mm and a repetition rate of 50% between adjacent spots. The laser power density  $I_0$  reaches  $3.82 \text{ GW/cm}^2$ . The laser shock treatment is illustrated in Fig. 1(a). A 40- $\mu\text{m}$ -thick Al foil was used as the absorption layer. A 2-mm-thick layer of water flowed over the surface of the Al foil to act as a confinement. During laser shocks, the laser beam was focused on the top of the Al foil via transparent water. High energy laser ionizes the Al foil and creates high-pressure plasma. The rapid expansion of the plasma induces a compressive shock wave into the sample [16]. In this process, the thermal effect of the plasma on samples can be effectively weakened by both Al foil and water layer. The stress amplitude of the shock wave can be estimated by the following relation [17,18]:

$$P_c = 0.01 \times \left( \frac{\lambda}{2\lambda + 3} \right)^{0.5} Z^{0.5} I_0^{0.5}, \quad (1)$$

where  $\lambda \sim 0.2$  is the internal energy conversion coefficient,  $Z \sim 2.03 \times 10^7 \text{ kg m}^{-2} \text{ s}^{-1}$  is the equivalent wave impedance related to Al foil and the sample. The calculated  $P_c$  is about 6.75 GPa, which is below the Hugoniot elastic limit

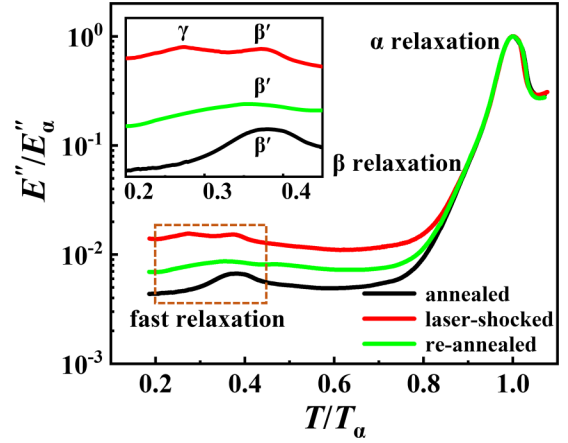


FIG. 2. Plots of the normalized loss modulus  $E''/E''_\alpha$  versus  $T/T_\alpha$  for the annealed, laser-shocked, and re-annealed samples. The inset is a magnification of the dashed box.

( $\sim 7 \text{ GPa}$ ) of Zr-based MGs [19–21]. In this situation, we prevented the introduction of any mechanical failure such as shear banding and crack into samples. Furthermore, some laser-shocked samples were annealed again at 653 K for 12 h to eliminate the effect of laser shocks as much as possible. Now we have three types of samples: annealed, laser-shocked, and re-annealed. The glassy structures of all samples were checked by x-ray diffraction (XRD), which showed typical diffuse scattering peaks, as seen in Fig. 1(b). The possibility of chemical separation and structural delamination of all samples was excluded by the energy dispersive spectroscopy (EDS) mappings, which is provided in Figs. S1–S4 of the Supplemental Material [22].

The relaxation behaviors of three types of samples were characterized by the TA Q800 DMA with a single-cantilever bending mode in a nitrogen-flushed atmosphere. The DMA tests were performed at driven frequencies of 1, 2, 4, and 6 Hz during continuous heating from 135 to 748 K with a constant heating rate of 3 K/min. The thermodynamic properties of samples were investigated by TA25 differential scanning calorimetry (DSC) and a Quantum Design physical property measuring system (PPMS). The structural changes were investigated by high-resolution transmission electron microscope (HRTEM) on a Cs-corrected JEM-2100F microscope and synchrotron high-energy XRD at the Beijing Synchrotron Radiation Facility. Nanoindentation measurements were tested by Nano Indenter G200 with Berkovich diamond indenter. The tests were performed at RT with a peak load  $P_{\text{max}}$  of 300 mN and a loading rate of 5 mN/s. The indent morphologies were scanned by Hysitron TriboScope atomic force microscopy (AFM).

### III. RESULTS AND DISCUSSION

#### A. Dynamic relaxation spectrums

Figure 2 shows the dynamic relaxation behaviors for the annealed, laser-shocked, and re-annealed samples at the driven frequency  $f = 1 \text{ Hz}$ . The ordinate (loss modulus  $E''$ ) and abscissa (test temperature  $T$ ) are scaled by the height  $E''_\alpha$  and temperature  $T_\alpha$  of the  $\alpha$  relaxation, respectively. In

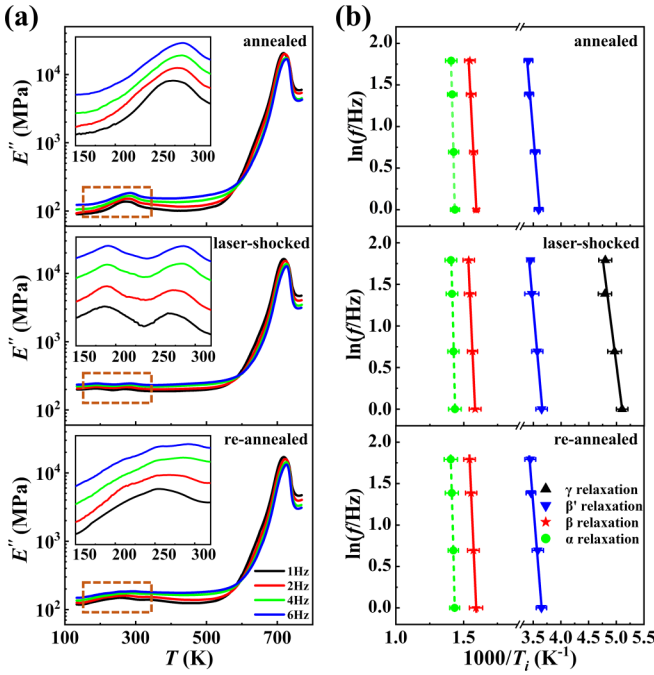


FIG. 3. (a) Temperature dependence of  $E''$  for the annealed, laser-shocked, and re-annealed samples tested at driven frequencies of 1, 2, 4, and 6 Hz. The inset is a magnification of the dashed box. (b) Plots of  $\ln(f)$  versus  $1000/T_i$  for the annealed, laser-shocked, and re-annealed samples. The black, blue, red, and green dots represent the  $\gamma$ ,  $\beta'$ ,  $\beta$ , and  $\alpha$  relaxations, respectively. The activation of the  $\gamma$ ,  $\beta'$ , and  $\beta$  relaxation follows the Arrhenius equation depicted by the solid lines, whereas that of the  $\alpha$  relaxation adheres to the VFT equation depicted by the dashed lines.

addition to the primary  $\alpha$  peak and the excess  $\beta$  wing, the fast relaxations appear below RT. However, the characteristics of the fast relaxations are very different in these samples (see the inset of Fig. 2), which is contrast to the almost unchanged  $\alpha$  and  $\beta$  relaxations. In the annealed sample, the fast relaxation manifests as a single  $\beta'$  peak with a height of  $0.007 E''_{\alpha}$  at  $0.37T_{\alpha}$ . In the laser-shocked sample, it is interesting to observe that the fast relaxation splits into two distinct peaks:  $\gamma$  at  $0.26T_{\alpha}$  and  $\beta'$  at  $0.38T_{\alpha}$ , but their heights are almost the same ( $\sim 0.016 E''_{\alpha}$ ). This implies that the  $\gamma$  and  $\beta'$  relaxations might share the similar structural origin. Further, this splitting phenomenon disappears in the re-annealed sample, and only the  $\beta'$  peak with a height of  $0.009 E''_{\alpha}$  survives at  $0.37T_{\alpha}$ . Such an observation of the switch of the fast relaxation between single- and two-peak in a fixed glassy system

should correspond to the reversible changes of structures in glasses.

Figure 3(a) presents the temperature dependence of  $E''$  at different driven frequencies  $f$  for the annealed, laser-shocked, and re-annealed samples. The insets enlarge the curves of the fast relaxations. The characteristic temperature  $T_i$  of the relaxations shifts to higher temperature with increasing  $f$ . The subset  $i$  in  $T_i$  denotes  $\gamma$ ,  $\beta'$ ,  $\beta$ , and  $\alpha$  relaxations, respectively. Based on this dependence, one can estimate the activation energy of the relaxations. For the fast and  $\beta$  relaxations, their activation usually follows the Arrhenius equation [2,23,24]:

$$f = f_0 \exp\left(\frac{-E_i}{k_B T_i}\right), \quad (2)$$

where  $f_0$  is the prefactor,  $E_i$  is the activation energy, and  $k_B$  is the Boltzmann constant. The Arrhenius fitting of the  $\ln(f)$  versus  $1/T_i$  data yields their activation energies  $E_i$ , as shown by the solid lines in Fig. 3(b). The activation of the  $\alpha$  relaxation is described by the Vogel-Fulcher-Tammann (VFT) equation [2,24,25]:

$$f = f_v \exp\left(-\frac{B}{T_i - T_0}\right), \quad (3)$$

where  $f_v \sim 3.98 \times 10^{14}$  Hz is the high-temperature relaxation frequency,  $B$  is the VFT parameter, and  $T_0$  is the VFT temperature. Both  $B$  and  $T_0$  are determined by the VFT fitting of the  $\ln(f)$  versus  $1/T_i$  data, as shown by the dashed lines in Fig. 3(b). The activation energy of the  $\alpha$  relaxation can be calculated as  $E_{\alpha} = -k_B B / (1 - T_0/T_{\alpha})^2$ . The results for  $E_i$  of all relaxations are summarized in Table I.

As shown in Table I, the values of both  $E_{\alpha}$  and  $E_{\beta}$  in three types of samples are almost unchanged. They are all larger than the values of the cast Vit105 MG [12,15], where  $E_{\alpha}$  is  $\sim 4.5$  eV, and  $E_{\beta}$  is  $\sim 1.6$  eV. Similar behavior was also observed by Chen *et al.* [26] in a  $\text{Zr}_{47.5}\text{Cu}_{47.5}\text{Al}_5$  metallic glass. They found that the as-cast  $\beta$  relaxation has an activation energy of  $\sim 1.9$  eV, but after a  $0.8T_g$  isothermal annealing the activation energy significantly increases to  $\sim 3.1$  eV. On the other hand, the values of both  $E_{\beta'}$  and  $E_{\gamma}$  are consistent with that of the cast sample [12,15]. This result is reasonable, because the prolonged annealing annihilates the excess free volume in samples. The laser shock treatment in our work does not introduce plastic deformation. So, the difference in the free volume of the three types of samples is not significant. Lower free volume hinders atomic cooperative motions and thus makes the  $\alpha$  and  $\beta$  relaxations more difficult to activate [26,27]. In comparison with  $\alpha$  and  $\beta$  relaxations, fast relaxations are suggested to originate from a more localized structure and do not involve the cooperative motions [8–12].

TABLE I. Activation energies of dynamic mechanical relaxations in the annealed, laser-shocked, and re-annealed samples.

| Activation energy (eV) | Fast relaxation     |                    |                          |                     |
|------------------------|---------------------|--------------------|--------------------------|---------------------|
|                        | $\alpha$ relaxation | $\beta$ relaxation | Fast $\beta'$ relaxation | $\gamma$ relaxation |
| Annealed               | $5.35 \pm 0.15$     | $3.31 \pm 0.15$    | $0.74 \pm 0.02$          |                     |
| Laser shocked          | $5.05 \pm 0.25$     | $3.25 \pm 0.05$    | $0.78 \pm 0.05$          | $0.47 \pm 0.09$     |
| Re-annealed            | $5.15 \pm 0.15$     | $3.25 \pm 0.12$    | $0.68 \pm 0.02$          |                     |

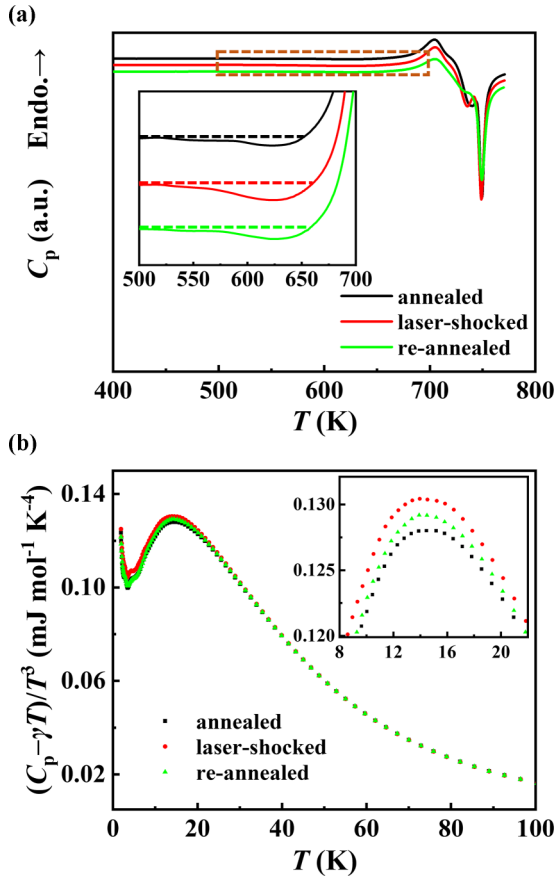


FIG. 4. (a) Specific heat capacity curves  $C_p$  of the annealed, laser-shocked, and re-annealed samples. The inset enlarges the changes of relaxation enthalpy before the glass transition. (b) Plots of  $(C_p - \gamma T)/T^3$  versus  $T$  between 1.9 and 100 K. The BPs' changes are highlighted in the inset.

So, the reduction in free volume caused by annealing has little effect on both  $E_{\beta'}$  and  $E_{\gamma}$ . The ratio of activation energies of  $\beta'$  and  $\beta$  relaxations decreases from the universal value  $\sim 0.5$  [12] to  $\sim 0.2$  for our annealed samples. Further, the  $E_{\gamma}$  is about  $2/3 E_{\beta'}$ , which is consistent with the finding of Shao *et al.* [11]. Smaller  $E_{\gamma}$  implies that the  $\gamma$  relaxation is related to more unstable structures than the  $\beta'$  relaxation.

### B. Thermodynamic properties

The specific heat capacity  $C_p$  curves of three types of samples are shown in Fig. 4(a). The relaxation enthalpy  $\Delta H_{\text{rel}}$  is determined by integrating the exothermic part before the glass transition as shown in the inset. The  $\Delta H_{\text{rel}}$  of the annealed, laser-shocked, and re-annealed samples are calculated to be  $0.037 \pm 0.01$ ,  $0.107 \pm 0.02$ , and  $0.047 \pm 0.01$  kJ/mol, respectively. The  $\Delta H_{\text{rel}}$  of the laser-shocked sample increases by about 0.07 kJ/mol compared to that of the annealed sample, indicating the occurrence of structural rejuvenation. However, the rejuvenation observed here is much weaker than those of the thermal cycling ( $\sim 0.65$  kJ/mol) [28], triaxial compression ( $\sim 1.08$  kJ/mol) [29], and high speed impact ( $\sim 1.32$  kJ/mol) [19]. When the laser-shocked sample is annealed again, its

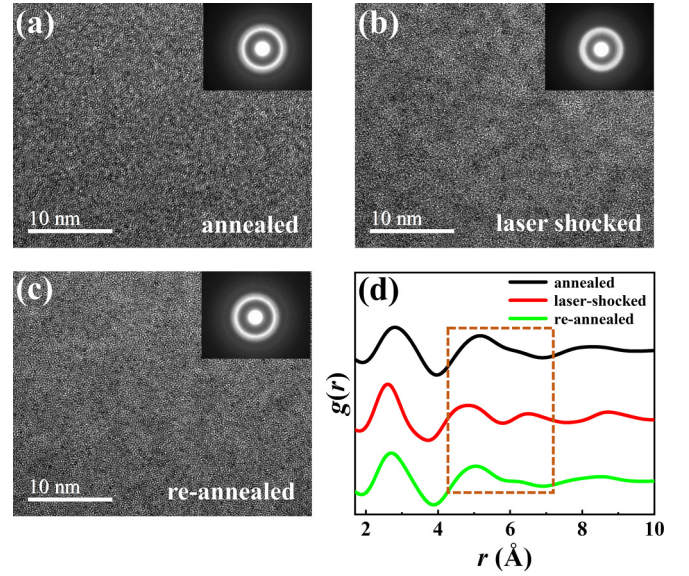


FIG. 5. (a)–(c) HRTEM images of the annealed, laser-shocked, and re-annealed samples, respectively. The insets show the corresponding SAED patterns. (d) RDFs deduced from the SAED patterns. The dashed box highlights the second-neighbor position.

$\Delta H_{\text{rel}}$  basically returned to the initial state within the error range.

We further characterize the vibrational dynamics of these samples. At terahertz frequencies, MGs exhibit excess vibrations over the Debye prediction, forming the boson peak (BP) [30]. These excess vibrations contribute to the enhancement of the low-temperature  $C_p$  as compared to the Debye  $T^3$  law [31,32]. For MGs, the low-temperature  $C_p$  contains the phononic and electronic contributions. The BPs can be visualized in the plot of  $(C_p - \gamma T)/T^3$  versus  $T$ , as shown in Fig. 4(b), where the Sommerfeld coefficient  $\gamma_s$  is determined by fitting  $C_p$  versus  $T^2$  below 8 K. As enlarged in the inset, the changes of BPs are consistent with those of relaxation enthalpy [Fig. 4(a)]. A slight increase of BP corresponds to the weak structural rejuvenation, which agrees well with the previous observations [19,32–35]. After re-annealing, the BP height decreases, partly recovered to its initial state. This slight rejuvenation observed here implies that the structural changes for the splitting of fast relaxation are very local, and re-annealing effectively eliminates such structural changes.

### C. Structural properties

HRTEM images of the annealed, laser-shocked, and re-annealed samples are shown in Figs. 5(a)–5(c). Typical long-range disordered, mazelike atom packing is observed, which corresponds to the halo ring selected-area electron diffraction (SAED) patterns shown in the insets. Through the quantitative analyses of SAED patterns [19,36,37], we obtain the radial distribution function (RDF)  $g(r)$  in real space, as shown in Fig. 5(d). The excess wing of the RDF's second peak is observed to transform into a bulge after the laser shock treatment. The bulge disappears in the re-annealed sample. These results demonstrate that the laser shocks reconstruct



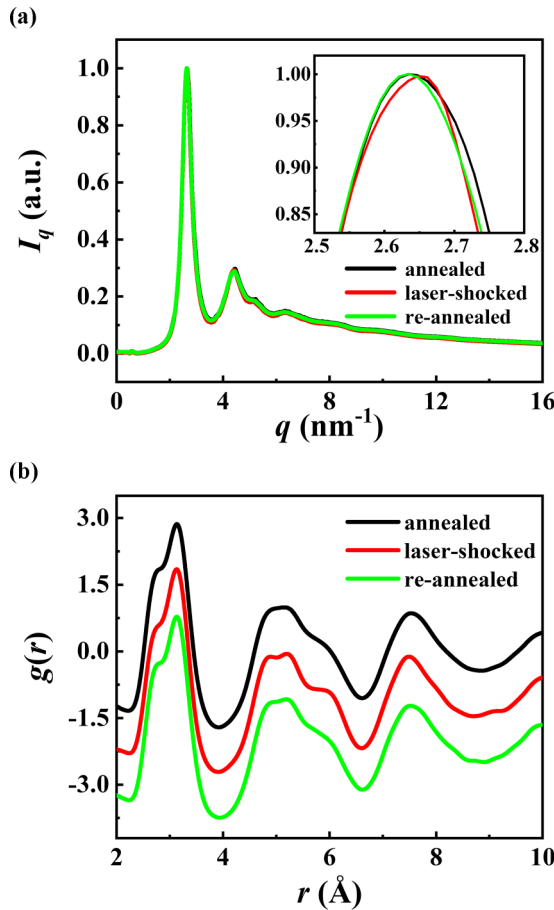


FIG. 6. High-energy XRD results for the annealed, laser-shocked, and re-annealed samples. (a) Diffraction intensity curves  $I(q)$ . The inset shows the local magnification of the upper portion of the first peaks. (b) RDF  $G(r)$  obtained by Fourier transformation of  $I(q)$  in (a).

the second-neighbor atoms in glassy structures. This MRO reconstruction should be responsible for the splitting of the fast relaxation. Such locally structural changes confirm that the observed relaxation splitting is a physical phenomenon rather than a technical issue.

We perform more precise examinations of the structural changes of samples with the synchrotron high-energy XRD. Figure 6(a) shows the diffraction intensity curves  $I(q)$  of the three types of samples. The inset shows the local magnification of the first peaks. We observe that, for the laser-shocked sample, its first peak slightly moves to right, indicating a decrease of the average atomic spacing. This behavior seems to contradict with the weak structural rejuvenation in Fig. 4. Similar phenomena were also observed in our previous work about the elastic compression of MGs [35,38,39]. In fact, this is rational due to two reasons. The first is that the present elastic shocks do not induce significant dilatation, and the latter usually occurs during the plastic deformation [40–42]. Second, the weak rejuvenation (or the splitting of fast relaxation) is ascribed to the MRO reconstruction [Fig. 5(d)]. To further confirm this, we perform the Fourier transformation of  $I(q)$  and obtain a higher spatial-resolution RDF shown in Fig. 6(b). The first RDF peaks, representing the short-range

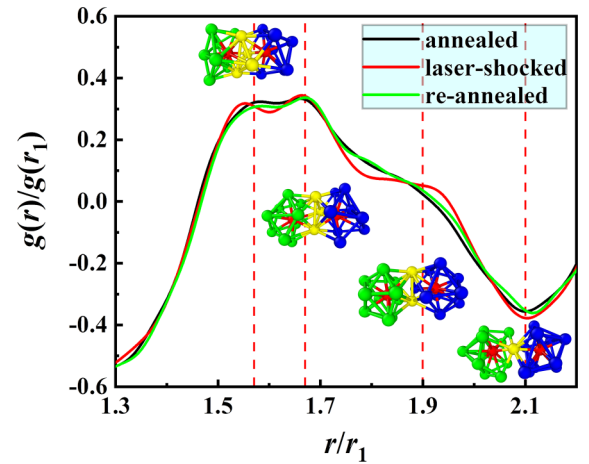


FIG. 7. Enlarged view of the second RDF peaks in Fig. 6(b). The ordinate and abscissa are respectively scaled by the height  $g(r_1)$  and position  $r_1$  of the first RDF peak. The vertical dashed lines mark the position of different MROs' types, which are interpenetrating ( $1.57r_1$ ), face sharing ( $1.66r_1$ ), edge sharing ( $1.90r_1$ ), and vertex sharing ( $2.10r_1$ ). The insets are the schematics of corresponding MROs' types. The red spheres represent the two central atoms that are second neighbor to each other. The green spheres belong to the left atomic clusters and the blue to the right. The yellow spheres are the sharing atoms of two atomic clusters.

order, are almost unchanged among the three types of samples. However, their second RDF peaks exhibit a noticeable variation, which is closely related to the reconfiguration of the MRO structures.

To show how the MROs reconstruct, Fig. 7 enlarges the view of the second RDF peaks in Fig. 6(b). The ordinate and abscissa are scaled by the height  $g(r_1)$  and position  $r_1$  of the first peak, respectively. Pan *et al.* [43] and Guo *et al.* [44] have extensively studied the MRO structures in MGs using atomistic simulations. According to their results, the second-neighbor atoms are of four types of connections: interpenetrating, face-sharing, edge-sharing, and vertex sharing with decreasing structural stability. These connection types are illustrated in Fig. 7, and their positions are marked by the vertical dashed lines. The interpenetrating connection is located at the left subpeak ( $1.57r_1$ ) of the second peak, while the right subpeak at  $1.66r_1$  corresponds to the face sharing. The excess wing at about  $1.90r_1$  denotes the edge sharing. The vertex-sharing connection is in the second valley at about  $2.10r_1$ , showing a negligibly low content. By comparison, we find that after the laser shocks, the left subpeak moves to the left, but the right subpeak is almost unchanged. The former should contribute to the right shift of the first diffraction peak [the inset of Fig. 6(a)]. Meanwhile, it is clearly seen that the excess wing transforms into an obvious shoulder. The subsequent re-annealing basically returns the MRO structures to its initially annealed state. These results demonstrate that the laser shocks exert a minimal influence on the interpenetrating and face-sharing MROs, but significantly increase the content of the edge-sharing MROs. Such MRO reconstructions well echo the splitting of the fast relaxations observed in Fig. 2. The  $\gamma$  relaxation, only presented in the laser-shocked sample,

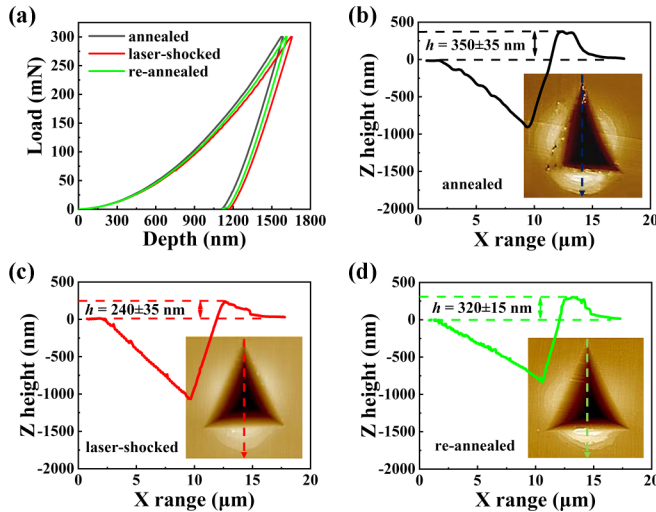


FIG. 8. Mechanical responses of the annealed, laser-shocked, and re-annealed samples to nanoindentation. (a) Load- and unload-depth curves. (b)–(d) AFM images of indents after unloading and the corresponding profiles along the downward dashed arrows.

arises from the unstable edge-sharing MROs. The  $\beta'$  relaxation, persistent in all samples, comes from the face-sharing and interpenetrating MROs. The activation of the MROs produces mechanical damping, possibly in the form of shaking modes. This gives rise to the fast relaxations on the dynamic relaxation spectrum. Compared with the face-sharing and interpenetrating types, edge-sharing MROs are more prone to shake due to their unstable connections. This explains why the activation energy of  $\gamma$  relaxation is smaller than that of  $\beta'$ . Due to the same MRO origin, their heights are close to each other. Our structural image of the fast relaxation also supports the previous simulation findings. The activation of the MROs facilitates the reversible motion of NN atoms [13] and the liquidlike diffusion [14].

In the strong glass forming system like the bulk Vit105 MG here, relatively stable interpenetrating, face-sharing structures dominate the MROs and are well coupled [45]. As shown in Fig. 7, these stable structures are topologically separated from the unstable vertex-sharing MROs. This provides the possibility for the splitting of fast relaxation from  $\beta'$  to  $\gamma$  and  $\beta'$ ; see Fig. 2. Considering the connection diversity of MRO structures [43–45], we expect that the fast relaxation may be split into more peaks by carefully introducing larger strains above elasticity. The MRO changes induced by heavy deformation were reported recently [46]. This interesting point deserves further investigations in the future, but is beyond the scope of this paper.

#### D. Nanoindentation responses

At last, we use nanoindentation to study the RT plasticity of the three types of samples. Figure 8(a) shows typical load- and unload-depth curves during indentation. At the fixed  $P_{\max}$  of 300 mN, the laser-shocked sample responds with the larger

depth, as compared to the annealed and re-annealed samples. After unloading, the residual depth shows the same trend. The Meyer hardness [47] of the annealed, laser-shocked, and re-annealed samples are calculated to be  $7.41 \pm 0.03$ ,  $6.52 \pm 0.03$ , and  $7.16 \pm 0.05$  GPa, respectively. These results indicate the better plasticity for the laser-shocked sample with the two-peak fast relaxation. Figures 8(b)–8(d) show the AFM images of residual indents and the corresponding profiles. The measured pileup  $h$  of the annealed, laser-shocked, and re-annealed samples are  $350 \pm 35$ ,  $240 \pm 35$ , and  $320 \pm 15$  nm, respectively. As shown in Fig. 8(c), the lower pileup is associated with the more homogeneous deformation, and less shear banding occurs in the laser-shocked sample. As shown in Figs. 8(b) and 8(d), the annealed and re-annealed samples with the higher pileup suffer pronounced shear bands. Similar phenomena have also observed previously [48,49]. From these results, we suggest that the split fast relaxations with more unstable MROs benefit the homogeneous activation of shear transformations in plastic deformation [8]. Recently, Shao *et al.* [11] have also found that exciting  $\gamma$  relaxation contributes to MG's plasticity at cryogenic temperatures.

#### IV. CONCLUSIONS

In this work, taking the Vit105 as a model glass, we present experimental observation that the single-peak fast relaxation ( $\beta'$ ) splits into two distinct peaks ( $\gamma$  and  $\beta'$  relaxations). Such dynamic splitting is achieved by the compressive stress wave due to laser shocks. The laser-shocked glass experiences slight structure rejuvenation, indicated by both relaxation enthalpy and boson-peak vibrational anomaly. Further synchrotron RDF analyses reveal that the splitting of fast relaxation stems from the structural reconfigurations on MRO scales. The  $\beta'$  relaxation is due to excitations of the face-sharing and interpenetrating MROs, while the  $\gamma$  relaxation is due to the unstable edge sharing. It is interesting to find that the isothermal annealing can recover the reconstructed MROs to their original state. The excitation of  $\gamma$  relaxation contributes to large-scale shear transformations, thus enhancing the RT plasticity of the laser-shocked glass. Our work demystifies the structural birth of the fast relaxation in MGs, and also offers the understanding of the effect of laser shock peening on plasticity of MGs [50,51] from the viewpoint of dynamic relaxations.

#### ACKNOWLEDGMENTS

This work was supported by the National Outstanding Youth Science Fund Project (Grant No. 12125206), Basic Science Center for “Multiscale Problems in Nonlinear Mechanics” (Grant No. 11988102), and General Project (Grant No. 11972345) of NSFC, CAS Project for Young Scientists in Basic Research (Project No. YSBR-096), and National Key Basic Research Program of China (Grant No. 2020YFA0406101).

- [1] M. Q. Jiang and L. H. Dai, Mechanics of amorphous solids, *Chin. Sci. Bull.* **67**, 2578 (2022).
- [2] W. H. Wang, Dynamic relaxations and relaxation-property relationships in metallic glasses, *Prog. Mater. Sci.* **106**, 100561 (2019).
- [3] H. B. Yu, R. Richert, and K. Samwer, Structural rearrangements governing Johari-Goldstein relaxations in metallic glasses, *Sci. Adv.* **3**, e1701577 (2017).
- [4] P. Luo, P. Wen, H. Y. Bai, B. Ruta, and W. H. Wang, Relaxation decoupling in metallic glasses at low temperatures, *Phys. Rev. Lett.* **118**, 225901 (2017).
- [5] J. C. Qiao, Y. J. Wang, L. Z. Zhao, L. H. Dai, D. Crespo, J. M. Pelletier, L. M. Keer, and Y. Yao, Transition from stress-driven to thermally activated stress relaxation in metallic glasses, *Phys. Rev. B* **94**, 104203 (2016).
- [6] B. Ruta, Y. Chushkin, G. Monaco, L. Cipolletti, E. Pineda, P. Bruna, V. M. Giordano, and M. Gonzalez-Silveira, Atomic-scale relaxation dynamics and aging in a metallic glass probed by x-ray photon correlation spectroscopy, *Phys. Rev. Lett.* **109**, 165701 (2012).
- [7] Y. Sun, S. X. Peng, Q. Yang, F. Zhang, M. H. Yang, C. Z. Wang, K. M. Ho, and H. B. Yu, Predicting complex relaxation processes in metallic glass, *Phys. Rev. Lett.* **123**, 105701 (2019).
- [8] Q. Wang, S. T. Zhang, Y. Yang, Y. D. Dong, C. T. Liu, and J. Lu, Unusual fast secondary relaxation in metallic glass, *Nat. Commun.* **6**, 7876 (2015).
- [9] S. Kuchemann and R. Maaß, Gamma relaxation in bulk metallic glasses, *Scr. Mater.* **137**, 5 (2017).
- [10] L. Z. Zhao, R. J. Xue, Z. G. Zhu, K. L. Ngai, W. H. Wang, and H. Y. Bai, A fast dynamic mode in rare earth based glasses, *J. Chem. Phys.* **144**, 204507 (2016).
- [11] L. Shao, L. Xue, J. Qiao, Q. Wang, Q. Wang, and B. Shen, Gamma relaxation in Dy-based metallic glasses and its correlation with plasticity, *Scr. Mater.* **222**, 115017 (2023).
- [12] Q. Wang, J. J. Liu, Y. F. Ye, T. T. Liu, S. Wang, C. T. Liu, J. Lu, and Y. Yang, Universal secondary relaxation and unusual brittle-to-ductile transition in metallic glasses, *Mater. Today* **20**, 293 (2017).
- [13] B. Wang, L. J. Wang, B. S. Shang, X. Q. Gao, Y. Yang, H. Y. Bai, M. X. Pan, W. H. Wang, and P. F. Guan, Revealing the ultra-low-temperature relaxation peak in a model metallic glass, *Acta Mater.* **195**, 611 (2020).
- [14] C. Chang, H. P. Zhang, R. Zhao, F. C. Li, P. Luo, M. Z. Li, and H. Y. Bai, Liquid-like atoms in dense-packed solid glasses, *Nat. Mater.* **21**, 1240 (2022).
- [15] N. Z. Zhang, X. L. Bian, C. Ren, C. Geng, Y. K. Mu, X. D. Ma, Y. D. Jia, Q. Wang, and G. Wang, Manipulation of relaxation processes in a metallic glass through cryogenic treatment, *J. Alloys Compd.* **894**, 162407 (2022).
- [16] X. Song, X. Q. Wu, K. L. Xiao, C. Li, H. Y. Wang, and M. Q. Jiang, Nanosecond laser ablation of a metallic glass in water: A high time-resolved imaging study, *Philos. Mag.* **100**, 2708 (2020).
- [17] R. Fabbro, J. Fournier, P. Ballard, D. Devaux, and J. Virmont, Physical study of laser-produced plasma in confined geometry, *J. Appl. Phys.* **68**, 775 (1990).
- [18] A. De Giacomo, M. Dell'Aglio, A. Santagata, R. Gaudiuso, O. De Pascale, P. Wagener, G. C. Messina, G. Compagnini, and S. Barcikowski, Cavitation dynamics of laser ablation of bulk and wire-shaped metals in water during nanoparticles production, *Phys. Chem. Chem. Phys.* **15**, 3083 (2013).
- [19] G. Ding, C. Li, A. Zaccone, W. H. Wang, H. C. Lei, F. Jiang, Z. Ling, and M. Q. Jiang, Ultrafast extreme rejuvenation of metallic glasses by shock compression, *Sci. Adv.* **5**, eaaw6249 (2019).
- [20] F. Xi, Y. Yu, C. Dai, Y. Zhang, and L. Cai, Shock compression response of a Zr-based bulk metallic glass up to 110 GPa, *J. Appl. Phys.* **108**, 083537 (2010).
- [21] B. Luo, G. Wang, F. Tan, J. Zhao, C. Liu, and C. Sun, Dynamic behaviors of a Zr-based bulk metallic glass under ramp wave and shock wave loading, *AIP Adv.* **5**, 067161 (2015).
- [22] See Supplemental Material at <http://link.aps.org/supplemental/10.1103/PhysRevB.109.024201> for the splitting of fast relaxations and the energy dispersive spectroscopy mapping of studied glasses.
- [23] H. B. Yu, W. H. Wang, H. Y. Bai, Y. Wu, and M. W. Chen, Relating activation of shear transformation zones to  $\beta$  relaxations in metallic glasses, *Phys. Rev. B* **81**, 220201(R) (2010).
- [24] J. C. Qiao, Q. Wang, J. M. Pelletier, H. Kato, R. Casalini, D. Crespo, E. Pineda, Y. Yao, and Y. Yang, Structural heterogeneities and mechanical behavior of amorphous alloys, *Prog. Mater. Sci.* **104**, 250 (2019).
- [25] J. C. Qiao and J. M. Pelletier, Dynamic universal characteristic of the main ( $\alpha$ ) relaxation in bulk metallic glasses, *J. Alloys Compd.* **589**, 263 (2014).
- [26] H. Chen, Y. Hai, R. Li, K. Sun, J. Xu, Y. G. Xia, G. Wang, and W. Yin, Defects controlled rejuvenation in the  $Zr_{47.5}Cu_{47.5}Al_5$  metallic glass, *J. Alloys Compd.* **927**, 166876 (2022).
- [27] S. Chen, S. Li, J. Ma, H. Yu, H. Liu, and H. Peng, Ultrasonic vibration accelerated aging in La-based bulk metallic glasses, *J. Non-Cryst. Solids* **535**, 119967 (2020).
- [28] S. V. Ketov, Y. H. Sun, S. Nachum, Z. Lu, A. Checchi, A. R. Beraldin, H. Y. Bai, W. H. Wang, D. V. Louzguine-Luzgin, M. A. Carpenter *et al.*, Rejuvenation of metallic glasses by non-affine thermal strain, *Nature (London)* **524**, 200 (2015).
- [29] J. Pan, Y. P. Ivanov, W. H. Zhou, Y. Li, and A. L. Greer, Strain-hardening and suppression of shear-banding in rejuvenated bulk metallic glass, *Nature (London)* **578**, 559 (2020).
- [30] J. Yang, Y. J. Wang, E. Ma, A. Zaccone, L. H. Dai, and M. Q. Jiang, Structural parameter of orientational order to predict the boson vibrational anomaly in glasses, *Phys. Rev. Lett.* **122**, 015501 (2019).
- [31] M. Q. Jiang, M. Peterlechner, Y. J. Wang, W. H. Wang, F. Jiang, L. H. Dai, and G. Wilde, Universal structural softening in metallic glasses indicated by boson heat capacity peak, *Appl. Phys. Lett.* **111**, 261901 (2017).
- [32] Y. Li, P. Yu, and H. Y. Bai, Observation of low-temperature specific-heat anomaly in CuZrAl bulk metallic glasses, *Appl. Phys. Lett.* **86**, 231909 (2005).
- [33] J. Bünz, T. Brink, K. Tsuchiya, F. Meng, G. Wilde, and K. Albe, Low temperature heat capacity of a severely deformed metallic glass, *Phys. Rev. Lett.* **112**, 135501 (2014).
- [34] H. Zhou, R. Hubek, M. Peterlechner, and G. Wilde, Two-stage rejuvenation and the correlation between rejuvenation behavior and the boson heat capacity peak of a bulk metallic glass, *Acta Mater.* **179**, 308 (2019).
- [35] Y. Gao, C. Yang, G. Ding, L.-H. Dai, and M.-Q. Jiang, Structural rejuvenation of a well-aged metallic glass, *Fundam. Res.* (2022), doi:10.1016/j.fmre.2022.12.004.

- [36] Y. M. Chen, T. Ohkubo, T. Mukai, and K. Hono, Structure of shear bands in Pd<sub>40</sub>Ni<sub>40</sub>P<sub>20</sub> bulk metallic glass, *J. Mater. Res.* **24**, 1 (2009).
- [37] J. Kim, H. S. Oh, J. Kim, C. W. Ryu, G. W. Lee, H. J. Chang, and E. S. Park, Utilization of high entropy alloy characteristics in Er-Gd-Y-Al-Co high entropy bulk metallic glass, *Acta Mater.* **155**, 350 (2018).
- [38] X. Sun, G. Ding, G. Mo, L. H. Dai, and M. Q. Jiang, Dilatancy signatures of amorphous plasticity probed by X-ray synchrotron radiation, *Intermetallics* **107**, 34 (2019).
- [39] Y. Gao, G. Ding, C. Yang, B. B. Zhang, C. J. Shi, L. H. Dai, and M. Q. Jiang, Rejuvenation-deformation relationship of a well-aged metallic glass during Newtonian to non-Newtonian flow, *J. Non-Cryst. Solids* **615**, 122410 (2023).
- [40] M. Q. Jiang, G. Wilde, and L. H. Dai, Origin of stress overshoot in amorphous solids, *Mech. Mater.* **81**, 72 (2015).
- [41] Y. Z. Lu, M. Q. Jiang, X. Lu, Z. X. Qin, Y. J. Huang, and J. Shen, Dilatancy of shear transformations in a colloidal glass, *Phys. Rev. Appl.* **9**, 014023 (2018).
- [42] X. J. Wang, Y. Z. Lu, X. Lu, J. T. Huo, Y. J. Wang, W. H. Wang, L. H. Dai, and M. Q. Jiang, Elastic criterion for shear-banding instability in amorphous solids, *Phys. Rev. E* **105**, 045003 (2022).
- [43] S. P. Pan, J. Y. Qin, W. M. Wang, and T. K. Gu, Origin of splitting of the second peak in the pair-distribution function for metallic glasses, *Phys. Rev. B* **84**, 092201 (2011).
- [44] Y. R. Guo, C. Qiao, J. J. Wang, H. Shen, S. Y. Wang, Y. X. Zheng, R. J. Zhang, L. Y. Chen, W.-S. Su, C. Z. Wang *et al.*, Bergman-type medium range order in amorphous Zr<sub>77</sub>Rh<sub>23</sub> alloy studied by *ab initio* molecular dynamics simulations, *J. Alloys Compd.* **790**, 675 (2019).
- [45] Z. W. Wu, M. Z. Li, W. H. Wang, and K. X. Liu, Hidden topological order and its correlation with glass-forming ability in metallic glasses, *Nat. Commun.* **6**, 6035 (2015).
- [46] K. Nomoto, B. Li, C. Gammer, A. V. Ceguerra, H. Bilal, A. Hohenwarter, J. Eckert, B. Gludovatz, S. P. Ringer, and J. J. Kruzic, Deformation-induced medium-range order changes in bulk metallic glasses, *Phys. Rev. Mater.* **6**, 043603 (2022).
- [47] M. C. Li, M. Q. Jiang, F. Jiang, L. He, and J. Sun, Testing effects on hardness of a Zr-based metallic glass under nanoindentation, *Scr. Mater.* **138**, 120 (2017).
- [48] H. Huang, J. Zhang, C.-H. Shek, and J. Yan, Effects of pre-compression deformation on nanoindentation response of Zr<sub>65</sub>Cu<sub>15</sub>Al<sub>10</sub>Ni<sub>10</sub> bulk metallic glass, *J. Alloys Compd.* **674**, 223 (2016).
- [49] J. Pan, Y. X. Wang, Q. Guo, D. Zhang, A. L. Greer, and Y. Li, Extreme rejuvenation and softening in a bulk metallic glass, *Nat. Commun.* **9**, 560 (2018).
- [50] J. Fu, Y. Zhu, C. Zheng, R. Liu, and Z. Ji, Effect of laser shock peening on mechanical properties of Zr-based bulk metallic glass, *Appl. Surf. Sci.* **313**, 692 (2014).
- [51] Y. Cao, X. Xie, J. Antonaglia, B. Winiarski, G. Wang, Y. C. Shin, P. J. Withers, K. A. Dahmen, and P. K. Liaw, Laser shock peening on Zr-based bulk metallic glass and its effect on plasticity: Experiment and modeling, *Sci. Rep.* **5**, 10789 (2015).